The Journal of Chemical Physics

^{15}N photo-CIDNP MAS NMR analysis of a bacterial photosynthetic reaction center of *Rhodobacter sphaeroides* wildtype

Cite as: J. Chem. Phys. **151**, 195101 (2019); https://doi.org/10.1063/1.5128783
Submitted: 23 September 2019 . Accepted: 23 October 2019 . Published Online: 18 November 2019

Shubhajit Paul, Upasana Roy, Michael Böckers, Johannes Neugebauer, A. Alia, and Jörg Matysik

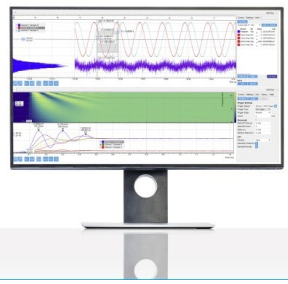

The Journal of Chemical Physics ARTICLE scitation.org/journal/jcp

^{15}N photo-CIDNP MAS NMR analysis of a bacterial photosynthetic reaction center of *Rhodobacter sphaeroides* wildtype

Cite as: J. Chem. Phys. 151, 195101 (2019); doi: 10.1063/1.5128783
Submitted: 23 September 2019 • Accepted: 23 October 2019 •
Published Online: 18 November 2019

Shubhajit Paul,[1] Upasana Roy,[1] Michael Böckers,[2] Johannes Neugebauer,[2] A. Alia,[3,4] and Jörg Matysik[1,a)]

AFFILIATIONS

[1]Institut für Analytische Chemie, Universität Leipzig, Linnéstr. 3, D-04103 Leipzig, Germany
[2]Organisch-Chemisches Institut and Center for Multiscale Theory and Computation, Universität Münster, Corrensstraße 40, D-48149 Münster, Germany
[3]Institut für Medizinische Physik und Biophysik, Universität Leipzig, Härtelstr. 16, D-04107 Leipzig, Germany
[4]Leiden Institute of Chemistry, Leiden University, Einsteinweg 55, P.O. Box 9502, 2300 RA Leiden, The Netherlands

Note: The paper is part of the JCP Special Topic on Spin Chemistry.
[a)]Author to whom correspondence should be addressed: joerg.matysik@uni-leipzig.de. **Tel.:** +49-341-9736112. **Fax:** +49-341-9736115.

ABSTRACT

The solid-state photochemically induced dynamic nuclear polarization (photo-CIDNP) effect has been studied in a quinone-depleted uniformly (u-)^{13}C,^{15}N-labeled photosynthetic reaction center (RC) protein from purple bacterium *Rhodobacter* (*R.*) *sphaeroides* wild type (WT). As a method for investigation, solid-state ^{15}N NMR under magic-angle spinning (MAS) is applied under both continuous illumination (steady state) and nanosecond-laser flashes (time-resolved). While all previous ^{15}N photo-CIDNP MAS NMR studies on the purple bacterial RC used the carotenoid-less mutant R26, this is the first using WT samples. The absence of further photo-CIDNP mechanisms (compared to R26) and various couplings (compared to ^{13}C NMR experiments on ^{13}C-labeled samples) allows the simplification of the spin-system. We report ^{15}N signals of the three cofactors forming the spin-correlated radical pair (SCRP) and, based on density-functional theory calculations, their assignment. The simulation of photo-CIDNP intensities and time-resolved ^{15}N photo-CIDNP MAS NMR data matches well to the frame of the mechanistic interpretation. Three spin-chemical processes, namely, radical pair mechanism, three spin mixing, and differential decay, generate emissive (negative) ^{15}N polarization in the singlet decay channel and absorptive (positive) polarization in the triplet decay channel of the SCRP. The absorptive ^{15}N polarization of the triplet decay channel is transiently obscured during the lifetime of the triplet state of the carotenoid (^{3}Car); therefore, the observed ^{15}N signals are strongly emissive. Upon decay of ^{3}Car, the transiently obscured polarization becomes visible by reducing the excess of emissive polarization. After the decline of ^{3}Car, the remaining nuclear hyperpolarization decays with nuclear T_1 relaxation kinetics.

I. INTRODUCTION

Photosynthetic reaction centers (RCs) can be referred to as light-driven electron pumps that convert light energy into chemical energy. In purple bacteria, photosynthesis occurs by light-induced electron transfer in the RC protein located in the intracytoplasmic membrane.[1] The RC (Fig. 1) of *Rhodobacter* (*R.*) *sphaeroides* wild type (WT) is a transmembrane protein complex consisting of a bacteriochlorophyll (BChl) dimer (P), called the "special pair" (P_L and P_M), which is the primary donor, accessory BChls, bacteriopheophytins (BPhe and Φ), quinones (Q), and a carotenoid (Car). Upon quinone-depletion, the electron-transfer pathway in *R. sphaeroides* becomes shorter and cyclic (Fig. 2):[2–5] Under illumination, the electron-transfer occurs from the photoexcited primary donor, the

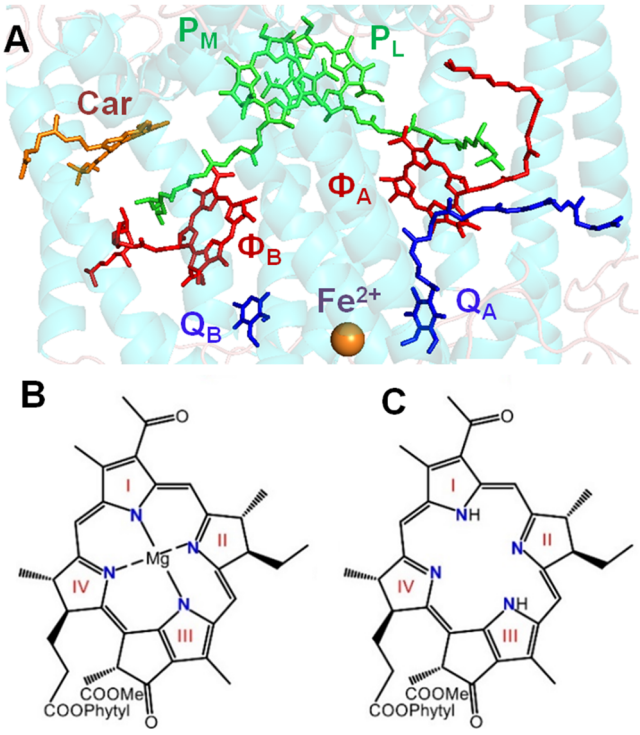

FIG. 1. (a) Spatial arrangement of cofactors of the bacterial reaction center (RC) of *Rhodobacter* (*R.*) *sphaeroides* [PDB entry 1M3X] wild type (WT) showing the primary electron donor, the "special pair" (P), formed by two bacteriochlorophylls *a* (P_L and P_M), the primary electron acceptor, a bacteriopheophytin *a* ($BPhe_A$ and Φ_A), the quinones Q_A and Q_B, and a carotenoid (Car). The chemical structures of BChl and BPhe are shown in (b) and (c), respectively.

special pair, P^*, to the primary BPhe acceptor Φ_A. As a result of this photoexcited electron transfer, a spin-correlated radical-pair (SCRP) is born in its pure singlet state $^S(P^{\bullet+}\Phi_A^{\bullet-})$. Its singlet-triplet interconversion is highly magnetic field dependent, and the reaction yield of both the singlet and triplet states of the SCRP depends on the field strength. It either evolves into a triplet state $^T(P^{\bullet+}\Phi_A^{\bullet-})$ via

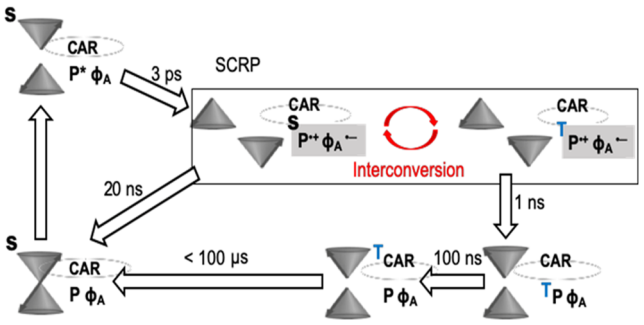

FIG. 2. The cyclic photo- and spin-chemical reaction scheme depicting formation and evolution of the spin-correlated radical-pair (SCRP) in quinone-depleted RCs of *R. sphaeroides* WT under conditions of natural abundance.

interconversion due to electron-electron spin interactions and hyperfine coupling with nearby nuclei or recombines to the singlet ground-state $^S(P\Phi_A)$. The triplet state cannot recombine although the electron back-transfer can occur by the formation of a molecular donor triplet state, ^TP. For WT RCs, the triplet donor state (^TP) is rapidly converted (100 ns) into a carotenoid triplet state (^{T}Car), followed by a much slower decay from the carotenoid triplet state to the electronic ground state (100 μs). During this cyclic electron transfer, photo-CIDNP (photochemically induced dynamic nuclear polarization) occurs, i.e., non-Boltzmann nuclear spin state distributions in the products of photochemical reactions, which is detected by NMR spectroscopy as either enhanced absorptive (positive) or emissive (negative) signals. In the solution state, the observed polarization in photo-CIDNP is due to the classical radical-pair mechanism (RPM) based on nuclear spin-sorting mediated by isotropic hyperfine coupling and difference of the *g*-values of the radicals.[6,7] In the solid state, the RPM can only be observed transiently in time-resolved experiments,[8,9] while under continuous illumination, the contributions of the two chemical branches cancel each other. However, in a rigid matrix, additional mechanisms are operational:[10] the three-spin mixing (TSM)[11,12] and the differential decay (DD)[13] mechanisms relying on electron-electron interactions. In the TSM mechanism, hyperfine coupling, nuclear and electronic Zeeman interactions, and anisotropic interactions involving electrons and nuclei lead to symmetry breaking and net nuclear polarization that can be observed both in laser-excitation experiments and under steady-state conditions. The DD mechanism relies on the different decay rates of SCRPs in the different spin multiplicities. These mechanisms require fulfillment of specific matching conditions depending, for example, on a particular architecture of spin states and a well-timed reaction kinetics as explored in magnetic field-dependent[14,15] and time-resolved[8,9] experiments. Since TSM contributions mostly dominate over those from DD, photo-CIDNP intensities reflect roughly local electron spin densities in the p_z-orbitals,[8,16,17] allowing the construction of pictures of molecular orbitals.[18] Recently, the solid-state mechanisms have been reinterpreted in terms of level-crossings and anticrossings.[19,20]

Several studies have been reported to understand the functional mechanism of these natural spin-machines using different NMR techniques in both soft[21] and solid states[9,14] and were mostly done on ^{13}C nuclei. These ^{13}C NMR studies are characterized by (i) crowded spectra particularly in the aromatic region causing difficulties for proper and accurate signal assignments, (ii) rather broad signals due to the homo- and heteronuclear dipolar coupling of ^{1}H and ^{13}C nuclei in the protein matrix (especially for the isotope-labeled systems), and (iii) spin-diffusion in the ^{1}H and ^{13}C networks in the protein membrane connected via several isotropic and anisotropic interactions (particularly in the isotope-labeled systems). Under these conditions, often two-dimensional separation experiments are required to allow for convincing signal assignment.[22] An alternative approach is the detection of ^{15}N nuclei in the hyperpolarized RCs. In many RCs, including those of "exotic" bacteria, ^{15}N isotope labeling is rather straightforward. The obtained 1D spectra show a selected number of signals, generally allowing the determination of the type and number of cofactors. ^{15}N photo-CIDNP MAS NMR studies on RCs of *R. sphaeroides* R26 (a mutant without carotenoid) were reported by Zysmilich and McDermott[23,24] and by us.[14,25,26] Furthermore, various other RCs were studied[17,27–29]

but not that of *R. sphaeroides* WT. While the analysis of R26 is more complex since a third mechanism producing photo-CIDNP is involved, called differential relaxation mechanism,[10,15] a WT sample appears to provide photo-CIDNP MAS NMR data that can be straightforwardly interpreted in terms of a SCRP formed by the two BChl *a* cofactors of the special pair as well of the Φ_A acceptor cofactor evolving according to the scheme shown in Fig. 2.

The present study relies on a WT sample containing uniform (u-)^{15}N as well as u-^{13}C isotope enrichment[30] studied under continuous illumination and with nanosecond laser flashes at 400-MHz using an NMR magnet (9.4 T). Theoretical simulations were carried out to obtain the ^{15}N chemical shifts as well as hyperfine coupling tensors. A main challenge might be the distinction of signals of the two donor cofactors that have been distinguished by ^{13}C photo-CIDNP MAS NMR.[31,32]

II. MATERIALS AND METHODS

A. Sample preparation

Cultures of *R. sphaeroides* WT were grown anaerobically on synthetic Potnat medium containing 3 g/l [u-^{13}C,^{15}N]-labeled algae hydrolysate. The cultures were allowed to grow for 7 days in light. For the preparation of RCs, the culture was centrifuged for 10 min at 5500 × *g* and the pellet was resuspended in 40 ml 0.1M phosphate buffer (pH = 7.5). The RCs were isolated as described by Shochat *et al.*[33] A protein/pigment ratio A_{280}/A_{802} = 1.2 was measured in the absorption spectrum to assess the purity of the samples. Approximately 5 mg of the RC protein complex embedded in LDAO micelles was used for NMR measurements. Prior to the NMR experiment, the RCs were reduced with 0.1M sodium dithionite and were loaded into a clear 4-mm sapphire rotor.

The [^{13}C,^{15}N]-isotope enrichment of the bacterial RC was measured by gas-chromatography and electron impact mass spectrometry (GC-MS). First, the proteins in the sample were hydrolyzed[34] followed by the derivatization of amino acids using the method of Ref. 35. The GC-MS was performed using a GC Chrompack 25 m fused silica column (CP-sil-5CB 0.25 mm id.; MS ITD 700, Finnigan MAT). Incorporation of [^{13}C,^{15}N]-isotopes in the RC complex was more than 90%.

B. NMR experiments

NMR experiments were performed with a 400 MHz (AVANCE-III) NMR spectrometer equipped with a double resonance CP/MAS probe (Bruker-Biospin, Karlsruhe, Germany). The sample was loaded into a clear 4-mm sapphire rotor and inserted into the magic-angle spinning (MAS) probe. The sample was frozen at a low spinning frequency of 1400 Hz to ensure a homogeneous sample distribution.[36] The light and dark spectra were collected using a Hahn-echo pulse sequence with the CYCLOPS phase cycle of the (π/2) pulse (Fig. S3). The data were collected with TPPM-15 proton decoupling[37] at a temperature of 252 K. The optimum length of the π/2 nitrogen pulse, determined on uniformly ^{15}N labeled histidine, is ~4.75 μs at a strength of 330 W. The rotational frequency for MAS was 8 kHz. The pulse sequence for time-resolved measurements using a laser has been used (see Fig. S1).

The ppm scale for histidine was calibrated with the known chemical shifts from the literature, which were referenced using external $^{15}NH_4Cl$, setting the ammonium peak to be 35.90 ppm downfield from that of liquid ammonia at −50 °C.[38] For ^{15}N photo-CIDNP MAS NMR experiments on u-^{13}C^{15}N labeled bacterial RCs of *R. sphaeroides* WT, the singlet of NΦ-IV at 297.26 ppm at a delay time of 0 μs was used for calibration.

C. Lamp setup

The continuous illumination setup for the MAS NMR experiments comprises a xenon arc lamp (1000 W, Müller Elektronik-Optik) with collimation optics, a liquid filter and glass filters, a focusing element, and a light fiber. Since the emission spectrum of a xenon lamp is similar to sunlight, the full range of radiation from UV to IR is available for illumination. Disturbance of the spinning frequency counting, which operates from a weak light source in the near-IR region, was avoided by a water filter as well as by various Schott filters such as WG320 and KG3. A fiber bundle was used to transfer the radiation from the collimation optics of the lamp to the sample.[25,39]

D. Flash laser setup

Using 1064-nm flashes of a Nd:YAG laser (Spectra-Physics Quanta-Ray INDI 40-10, Irvine CA, USA) and frequency-doubling with a second harmonic generator, 532-nm laser flashes were generated with pulse length 6–8 ns and an energy between 20 and 270 mJ. The laser was operated with a repetition frequency of 15 Hz. The pump lamp of the laser was triggered by the triggering impulse from the spectrometer. The delay between the lamp trigger and the laser output (Q-switch mode) was measured to be 237 μs using a 500-MHz oscilloscope (Series TDS3000B, Tektronix, Beaverton, USA). Channel 1 of the oscilloscope and the lamp trigger channel (of the laser power-supply) were connected in parallel to the transistor-transistor logic (TTL) channel of the spectrometer. Channel 2 of the oscilloscope was connected with the Q-switch sync (of the laser power supply). At the fiber output, the energy of a laser pulse was ~50 mJ.

E. Optical coupling of laser and NMR

Radiation emitted by the laser is transferred to the sample via a fiber bundle (FiberTech GmbH, Berlin, Germany). A multimode light fiber bundle provides high optical transparency in a broad spectral range as well as sufficient mechanical flexibility for being attached to the stator of the MAS probe. The optically active diameter is 3 mm, and the numerical aperture is 0.22. The ratio of the radiation energies between input and output powers of the fiber bundle is about 0.25. A Galilean lens system and a multimode fiber aligner are used for coupling the radiation pulses to the fiber bundle. The Galilean lens system, combining a concave lens with a convex one, allows collimation of the beam to the diameter required. The MAS NMR probe head (AVANCE-III, Bruker Biospin GmbH, Karlsruhe, Germany) has been modified in order to illuminate the rotor from the side.[25,39] This includes (a) a bore drilled into the most upper partition plate separating stator chamber and electronics, (b) drilling a small opening into the stator, and (c) winding a new coil from thin silver wire.

F. Chemical shift calculations

All calculations were performed using the Amsterdam density functional (ADF) program package (SCM N.V.).[40–46] The geometries for BPhe and the special pair (including all molecules consisting of at least one atom closer than 3.4 Å for the special pair and 3.5 Å for BPhe to any atom within the molecule of interest, in the following denoted as r34 and r35, respectively) were extracted from the Protein Data Bank (PDB ID: 1M3X), missing hydrogen atoms were added, and cleaved protein bonds were saturated with neutral groups $-C(O)CH_3$ and $-NH_2$ as the N- and C-terminus, respectively. The bond length of C- and N-termini was set to the average value of the respective distances in the crystal structure. The position of the hydrogen atoms was optimized using the DFTB3/3OB[47,48] method, as implemented in the ADF. For the closest residue models, all but the closest residues of the r34 and r35 models were removed without further optimization. Similarly, the isolated models were obtained by removing all residues. ^{15}N nuclear magnetic shieldings were calculated using the KT2 exchange-correlation functional[48] and a polarized triple zeta basis (TZP).[48] The numerical quality for the density fit and grid construction procedures were set to "very good," and tight convergence criteria were applied throughout (10^{-8} a.u. for the norm of the commutator of Fock and density matrix). Chemical shifts were calculated with respect to the NH_3 shieldings obtained with the same settings as described above and were shifted by 23.5 ppm for better comparability.

G. Calculation of hyperfine coupling tensors

Density-functional theory (DFT) computations of hyperfine coupling tensors were performed with the ADF 2002 package using the TZP basis set with polarization functions on all-electron basis set for all atoms as described.[11] Geometries of ground state molecules were taken from the crystal structure in the charge-neutral state[49] and subjected to geometry optimization within the ADF in the cation radical state *in vacuo*.

H. Solid-state photo-CIDNP intensity simulations

Numerical simulations of the photo-CIDNP effect on intensities are based on the theory described by Jeschke and Matysik,[10] implemented in the Matlab program (Jeschke, courtesy) for density matrix computation using the EasySpin library.[50] The program starts from a pure singlet state of the radical pair and computes the time evolution of the system using a Hamiltonian that includes electron Zeeman, nuclear Zeeman, and hyperfine interaction as well as dipole-dipole and exchange coupling between the two electron spins. The part of the density matrix that represents decay channels to the ground-state from either singlet or triplet radical pairs is projected out (diamagnetic part) and is further evaluated using a Hamiltonian including only the nuclear Zeeman interaction. Evolution is continued until the radical pairs have completely decayed (100 ns), and after that, the nuclear polarization of the diamagnetic part of the density matrix is determined. As an extension to the approach described by Jeschke and Matysik,[10] this procedure is performed for a full powder average, describing all interactions by tensors, except for the nuclear Zeeman interaction.

III. RESULTS AND DISCUSSION

A. Steady-state ^{15}N photo-CIDNP MAS NMR

Experiments performed at 9.4 T by illuminating with a xenon lamp are presented in Fig. 3. In the dark spectrum [Fig. 3(A)], only the features of the amide backbone and amino acids occur and

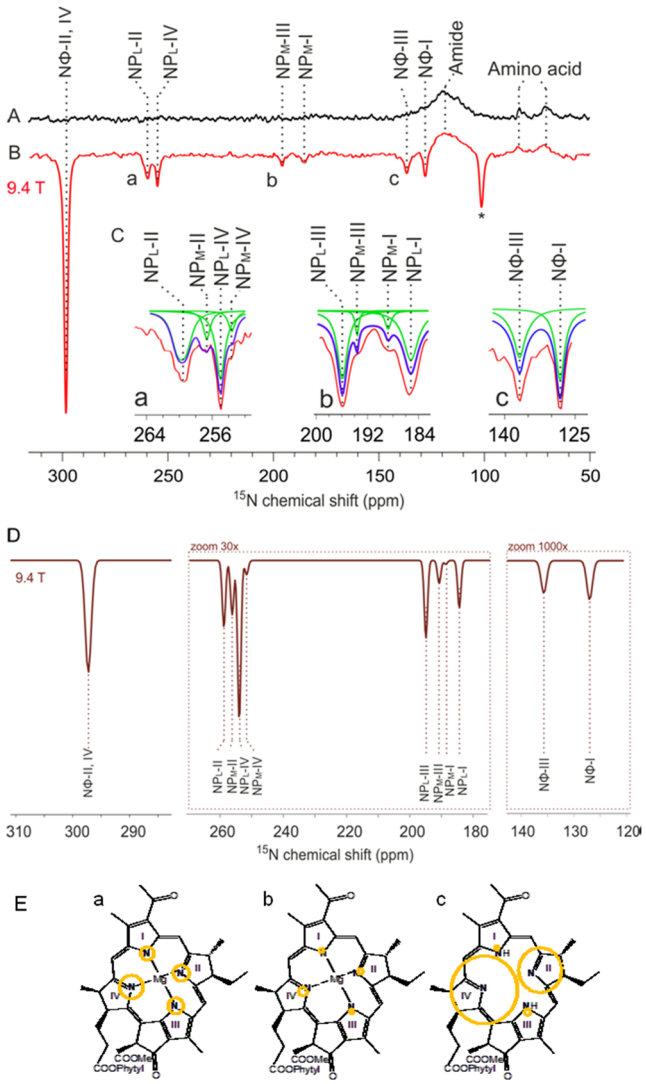

FIG. 3. ^{15}N MAS NMR spectra of u-^{13}C,^{15}N labeled RCs of *R. sphaeroides* WT obtained (A) in the dark and (B) under continuous illumination with a white lamp, at a temperature of 250 K, a MAS frequency of 8 kHz, and a magnetic field of 9.4 T. (C) The fitting of experimentally obtained ^{15}N photo-CIDNP MAS NMR spectra (red trace) has been made with Lorentz functions (green traces) of the same linewidth. The sum of all fitted peaks in the spectrum is given in blue. (D) Simulated ^{15}N photo-CIDNP MAS NMR spectra corresponding to polarization generated in a single photocycle. The theoretically simulated intensities have been linked to the tentatively assigned chemicals shifts (Table I). (E) Semiquantitative representation of the ^{15}N photo-CIDNP intensities for the different nitrogen positions: (a) P_L, (b) P_M, and (c) Φ_A.

provide an internal reference. The steady-state ^{15}N photo-CIDNP MAS NMR spectrum obtained under continuous illumination with the white light of a xenon lamp is presented in Fig. 3(B). The weak and broad positive hump arising at about 120 ppm originates from amide nitrogens of the protein backbone, and also the signals of the amino acids are well resolved. These proteins signals, which are not light-induced, demonstrate that all the light-induced signals are emissive (negative). The emissive sign is in line with previous observations[23,24,26] in both polarizing magnetic field strengths of 4.7 and 9.6 T. The light induced signals are confined in the region of 120–300 ppm. Some light-induced signals appear to be composed by overlying lines, and the enlarged images are shown in Fig. 3(C).

B. Signal assignment

In ^{15}N photo-CIDNP MAS NMR experiments under continuous illumination, due to weak coupling, spin-diffusion is not expected to equilibrate signal intensities; therefore, the observed intensities are related to local electron spin densities. Hence, signal assignment can be based on both chemical shifts and photo-CIDNP intensities. Chemical shifts are available from model compounds as well as from theoretical calculations (Table I). The simulated photo-CIDNP intensities [Fig. 3(D)] are related to the calculated values of the electron spin density in the p_z-orbitals, A_{zz} (Tables S1 to S3).

Up to 12 nitrogen signals are expected to occur. It is obvious that the signals of BPhe (Φ) are well distinguished from the signals of the special pair cofactors P_L and P_M. The outer three signals (297.26, 135.71, and 127.01 ppm) belong to Φ, while the inner ones originate from both P_L and P_M. The signals originating from the Φ acceptor are stronger than those from the special pair donor P. That difference might be due to the different localizations of the molecular orbitals. In a simple orbital picture, the spin density is localized in the (now singly occupied) LUMO of the acceptor and in the HOMO of the donor. The highest intensity is found at the signal at 297.26 ppm, which can be fitted with a single Lorentzian component. The chemical shift matches very well to that of NΦ-II, which is also expected to have a strong signal. The question arises whether this signal also contains the intensity of NΦ-IV, which is also expected to be high. Lacking an alternative, we tentatively assign the intense signal at 297.26 ppm to both NΦ-II and NΦ-IV. For the first time, the resonances from NΦ-I (127.01 ppm) and NΦ-III (135.71 ppm) have been observed in a bacterial RC, which can be assigned straightforwardly. The emissive peak at 101.36 ppm (labeled by asterisk) is a first-order spinning sideband for the peak at 297.26 ppm.

The ^{15}N photo-CIDNP MAS NMR spectrum [Fig. 3(B)] is expanded and fitted with Lorentz functions [Fig. 3(C)] to provide detailed insight into the assignment. Between 265 and 250 ppm [inset (a)], four signals can be clearly identified, which originate from the nitrogens NP-II and NP-IV. Their chemical shifts are very similar, although N-II is generally at slightly higher ppm-values than N-IV. Furthermore, the electron spin density is higher on P_L compared to P_M.[14,51] On that basis, we assign the signals at 261.9, 259.6, 254.9, and 252.7 ppm to NP_L-II, NP_M-II, NP_L-IV, and NP_M-IV, respectively.

In the range from 200 to 180 ppm [inset (b)], again four signals can be separated, originating from the nitrogens N-II and N-IV of P_L and P_M. Also here apply the general tendency that N-III resonates at higher ppm-values as N-II. Taken the higher spin density on P_L into account, too, we assign the signals 199.25, 191.10,

TABLE I. ^{15}N chemical shifts (experimentally measured and theoretically calculated) of BChl and BPhe of u-^{13}C^{15}N labeled bacterial reaction centers of *Rhodobacter sphaeroides* WT.

		Experimental ^{15}N chemical shifts (ppm) obtained on model compounds			Calculated ^{15}N chemical shifts (ppm) (including 23.5 ppm offset)		
IUPAC number	^{15}N chemical shifts (ppm) in this work (Expt.)	Solution state in acetone-d_6[a]	Solid state[b]	Solution state in acetone[c]	Isolated	Closest residue	r34/r35
NP_L-I	184.77	192.63	191.76	189.6	189.4	191.7	192.1
NP_M-I	189.04				189.8	192.5	192.5
NP_L-II	258.70	259.14	258.28	258.5	251.6	257.4	259.0
NP_M-II	251.57				250.8	252.9	253.3
NP_L-III	195.25	194.46	196.87	191.5	178.7	183.2	184.7
NP_M-III	191.10				178.2	182.4	182.9
NP_L-IV	253.87	261.71	258.28	259.1	253.1	258.1	257.3
NP_M-IV	256.10				252.0	261.7	261.4
NΦ-I	127.01	129.4	127.2		130.5	129.8	154.1
NΦ-II	297.26	299.2	296.07		302.3	302.2	330.2
NΦ-III	135.71	135.7	132.5		129.1	133.8	159.2
NΦ-IV	297.26	308.3	303.17		310.0	308.1	329.3

[a]Values of the nitrogen chemical shift (in ppm) in the solution-state in acetone-d_6 (from Ref. 54).
[b]Values of the nitrogen chemical shift (in ppm) in the solid-state (from Ref. 54).
[c]Values of the nitrogen chemical shift (in ppm) in acetone (from Ref. 55).

189.04, and 184.77 ppm to NP_L-III, NP_M-III, NP_M-I, and NP_L-I, respectively.

C. Simulated ^{15}N photo-CIDNP MAS NMR spectrum

To investigate the applicability of the theory of the solid-state photo-CIDNP effect,[10,12] we have simulated the ^{15}N photo-CIDNP MAS NMR spectrum [Fig. 3(B)] on the basis of the obtained chemical shift assignments. Using density functional theory (DFT) calculations, the complete hyperfine tensors (isotropic and anisotropic contribution and eigenvectors) were obtained (Tables S1 to S3). Based on the theory, ^{15}N photo-CIDNP MAS NMR spectra have been simulated for 9.4 T under continuous illumination. A reasonable agreement between experiment and simulation has been observed [Fig. 3(D)]. On that basis, the local electron spin densities are shown in Fig. 3(E) for P_L, P_M, and Φ.

D. Time-resolved ^{15}N photo-CIDNP MAS NMR

A spectrum, recorded for a delay time (Δ) of 0 μs after a 532-nm nanosecond laser flash, is presented in Fig. 4(B). The delay time Δ is defined as the duration between the laser-pulse and the beginning of the detection spin-echo radio-frequency pulse train. The pulse-sequence (Fig. S3C) contains three initial π/2 pulses for presaturation, i.e., to suppress the Boltzmann polarization prior to the laser pulse. The spectrum in Fig. 4(A) represents the dark spectrum that does not indicate any signal since the presaturation pulses are suppressing the Boltzmann polarization entirely.

The time-resolved spectrum [Fig. 4(B)] shows signals at the same ppm-values but with modified intensities compared to the steady-state spectrum [Fig. 3(B)]. In particular, the signals of NΦ-I (127.01 ppm) and NΦ-III (135.71 ppm) do not appear. In this section, between 200 and 180 ppm [Fig. 4(C), inset (b)], the intensity pattern might be changed. The difference in the intensity

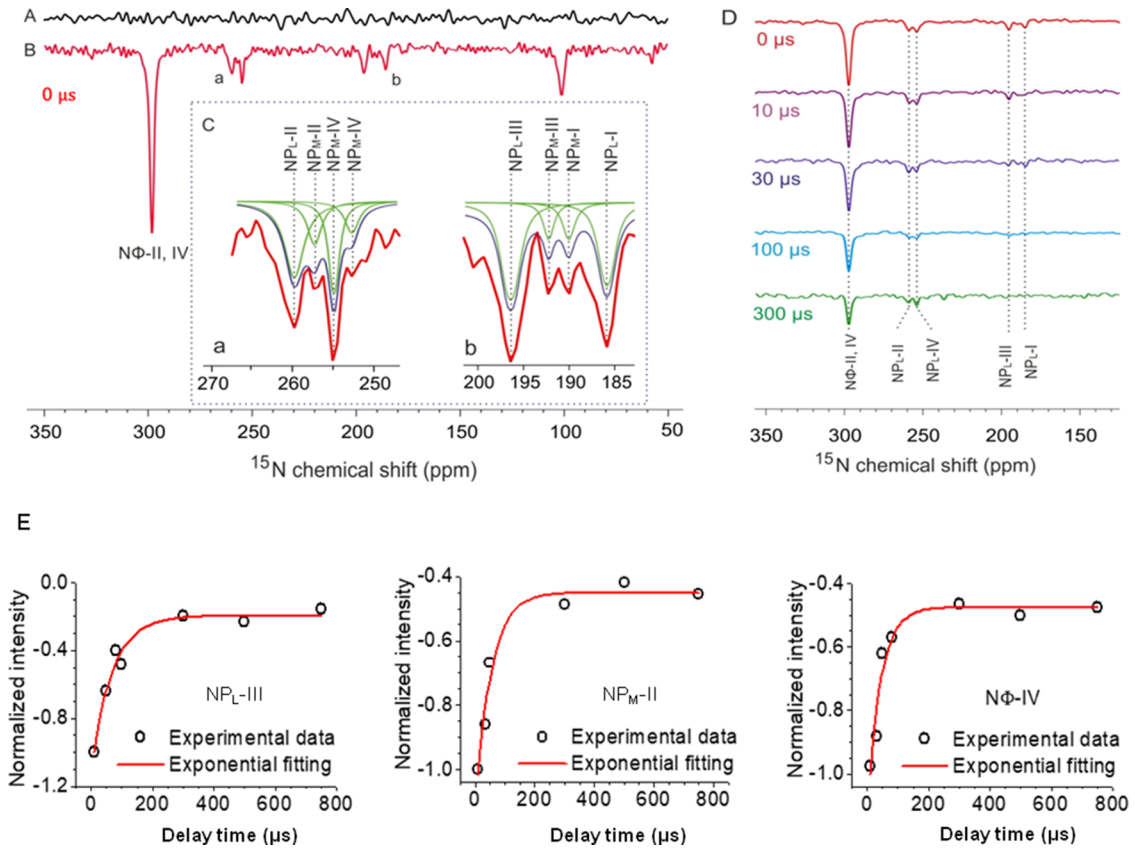

FIG. 4. Time-resolved ^{15}N MAS NMR spectra of u-^{13}C,^{15}N-labeled RCs of *R. sphaeroides* WT obtained in the (A) dark and (B) upon laser flash (532 nm, 8 ns) with 0 μs time delay (Δ) between the light pulse and the rf pulse. (C) The fitting of experimentally obtained ^{15}N photo-CIDNP MAS NMR spectra (red trace) with the Lorentzian function (green traces) of the same linewidth. The sum of all fitted peaks in the spectrum is given in blue. (D) Time-resolved ^{15}N photo-CIDNP MAS NMR spectra of u-^{13}C,^{15}N-labeled RC of *R. sphaeroides* WT obtained with laser flash (532 nm, 8 ns) with three selected time delays (Δ) between the light pulse and the rf pulse: (i) 0 μs, (ii) 10 μs, (iii) 30 μs, (iv) 100 μs, and (v) 300 μs. All spectra have been recorded at a magnetic field of 9.4 T and a temperature of 250 K. The MAS frequency was 8 kHz. The presaturation-based pulse-sequence used to obtain the spectra is shown in the supplementary material (Fig. S3). (E) Normalized intensities plotted as a function of the delay time Δ between the light pulse and the rf pulse for selected ^{15}N resonances from u-^{13}C,^{15}N-labeled *R. sphaeroides* WT. Details of the fitting parameters are given in Table S4.

pattern is due to the difference in the enhancement mechanism. While in steady-state experiments under continuous illumination, intensities are related to TSM and DD, in the early phase of time-resolved experiments obtained with laser flashes, the intensity relies on the RPM mechanism and therefore on the isotropic hyperfine interaction, A_{iso}. We assume that the spectrum shown in Fig. 4(B) contains some admixture of RPM contributions. According to the calculated values of A_{iso}, NΦ-I and NΦ-III are expected to have intensity similar to NP_M-I, which is also close to the noise level.

E. Evolution of the nuclear polarization

Time-resolved ^{15}N photo-CIDNP MAS NMR spectra were recorded for the delay times (Δ) of 0, 10, 30, 100, and 300 μs between the laser pulse and the detection radio-frequency pulses, which are presented in Fig. 4(D). With the increase in the delay time, a decrease in emissive signal intensity is apparent from the spectra. Hence, at Δ = 0 μs, the light-induced emissive nuclear hyperpolarization is at its maximum. The kinetics of the decay of nuclear hyperpolarization of selected nitrogens from both donor and acceptor sites is presented in Fig. 4(E) for three selected nitrogen positions. The experimentally obtained kinetic data are fitted with exponential decay functions. Details of the fitting procedure and the parameters are given in Table S4 of the supplementary material. The kinetic analysis shows a decay of a single component roughly on the time scale of the lifetime of the triplet state of the carotenoid, which is around 100 μs (Fig. 2).

Interestingly, the linewidth of the nitrogen signals is narrow and typical for ^{15}N MAS NMR on proteins (less than 100 Hz). Hence, no signal broadening by paramagnetic effects or fast relaxation is observed. These emissive signals originate from the singlet branch of the radical pair. In the RCs, undergoing recombination from the singlet state of the radical pair, no paramagnetic state occurs. Therefore, the initial signal has maximum emissive intensity. At that point of time, the positive polarization originating from the triplet branch of the radical pair is obscured by the nearby carotenoid triplet. This transiently obscured polarization (TOP) has been observed previously by time-resolved ^{13}C photo-CIDNP MAS NMR on a selectively ^{13}C labeled RC sample.[8]

Hence, the observed ^{15}N signals, showing the excess of the emissive polarization over the absorptive polarization, originate from the diamagnetic RCs. Since the nuclear T_1 in a frozen diamagnetic protein is on the time scale of several tens of seconds, polarization can be detected after several milliseconds (Fig. S2). In addition, in a study on RCs of *Rhodobacter sphaeroides* R26, ^{15}N polarization has been observed with 500 ms delay after the laser excitation.[26]

When the triplet state on the carotenoid decays, the TOP effect weakens and the absorptive nuclear polarization becomes visible by reducing the excess of the emissive nuclear polarization. The acceptor is significantly more distant to the carotenoid (about 25 Å), compared to the distance of P_M and P_L to the carotenoid (about 10 Å and 12 Å, respectively). Therefore, the TOP effect is less efficient on the acceptor, the increase in absorptive polarization is faster, and the decay of the excess emissive nuclear magnetization is faster [Fig. 4(E)].

Thus, the observed data obtained from a uniformly ^{15}N-labeled WT sample can be well explained within the framework of theory built up on ^{13}C experiments or ^{15}N-experiments on R26-RCs. Now, we will use this theory to predict optimized conditions for future experiments.

F. Magnetic field dependence of the solid-state ^{15}N photo-CIDNP effect

The effect of the magnetic field strength on the photo-CIDNP MAS NMR intensities, obtained by theoretical simulations, is shown in Fig. 5 (normalized with respect to the maxima correspond to NΦ-IV) for various ^{15}N nuclei of the special pair [Fig. 5(a)] and the acceptor $BPhe_A$ [Fig. 5(b)] (details of the simulations are given in the supplementary material). These enhancement curves show a global maximum at ≈2 T (85 MHz ^{1}H frequency). In the field region applied in the present work (9.4 T), the photo-CIDNP enhancement is simulated to be emissive (negative), as observed, with a local minimum at ≈7.5 T (320 MHz ^{1}H frequency). Hence, this study suggests the strong ^{15}N nuclear polarization at fields below 1 T, which might be accessible by a shuttle MAS NMR experiment.[56]

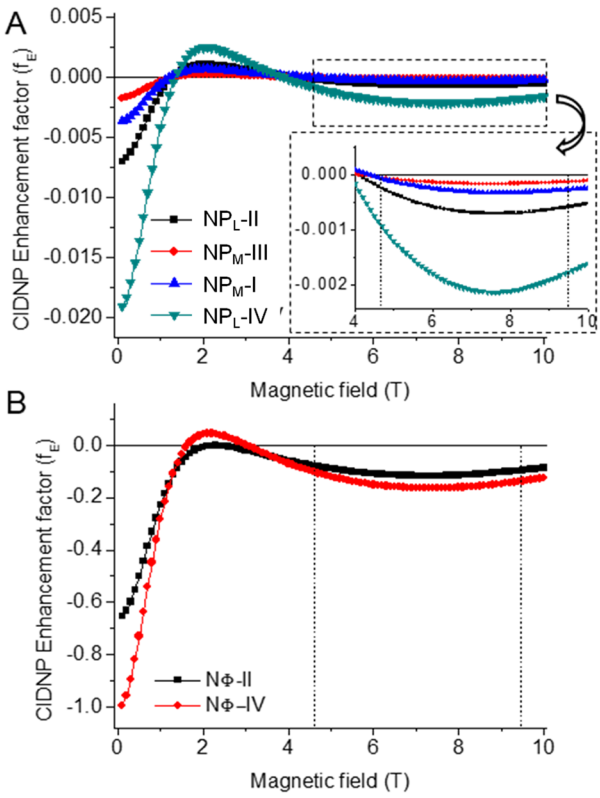

FIG. 5. Simulated magnetic-field dependence of ^{15}N NMR solid-state photo-CIDNP enhancement (f_E) in the high-field range for selected nitrogens from the donor special pair (P) and acceptor pheophytin ($BPhe_A$): (a) NP_L-II, NP_M-III, NP_M-I, and NP_L-IV and (b) NΦ-II and NΦ-IV. The computed enhancement factors refer to photo-CIDNP/thermal polarization and are normalized with respect to the maximum, observed for NΦ-IV. Computed values are plotted as marker symbols, connected by lines to guide the eye.

IV. CONCLUSIONS

In previous studies of the ^{15}N solid-state photo-CIDNP effect in RCs of *R. sphaeroides*,[23,24,26,52,53] the carotenoid-less mutant R26 was used in which the spin-dynamics mechanism is more complex. Here, we report the effect in WT RCs. In these WT RCs, we show steady-state and time-resolved ^{15}N photo-CIDNP MAS NMR data with theoretical simulations for magnetic field dependence of photo-CIDNP. The results match well with the present interpretation of a SCRP formed by the special pair and $BPhe_A$, producing nuclear spin hyperpolarization via RPM, TSM, and DD, and the TOP effect. Analysis of the same u-^{13}C^{15}N labeled sample by ^{13}C photo-CIDNP MAS NMR was impeded by the omnipresence of ^{13}C–^{13}C couplings.[30] Hence, results obtained on this "minimum system," having neglectable couplings and no contributions by the DR effect, are in line with the present theory.

SUPPLEMENTARY MATERIAL

See the supplementary material for the experimental setup, the DFT calculations, kinetic fitting of the decay curve, and ^{15}N photo-CIDNP MAS spectra obtained at 1 and 50 ms delay.

ACKNOWLEDGMENTS

The authors gratefully acknowledge the financial support received from The Netherlands Organisation for Scientific Research (NWO, Grant No. 818.02.019) and the Deutsche Forschungsgemeinschaft (DFG, Grant Nos. MA 497/2-1 and MA 497/11-1). The authors are thankful to Mr. Patrick Eschenbach for the generation and optimization of the model structures and Professor Gunnar Jeschke (ETH Zürich), Dr. Chen Song (Univ. Leipzig), and two unknown reviewers for helpful discussions.

The authors declare no competing financial interests.

REFERENCES

[1] X. Hu *et al.*, Q. Rev. Biophys. **35**, 1 (2002).
[2] C. A. Dodson, P. J. Hore, and M. I. Wallace, Trends Biochem. Sci. **38**, 435 (2013).
[3] A. J. Hoff, Q. Rev. Biophys. **14**, 599 (2009).
[4] R. E. Blankenship, T. J. Schaafsma, and W. W. Parson, Biochim. Biophys. Acta, Bioenerg. **461**, 297 (1977).
[5] A. J. Hoff *et al.*, Biochim. Biophys. Acta, Bioenerg. **460**, 547 (1977).
[6] G. L. Closs and L. E. Closs, J. Am. Chem. Soc. **91**, 4549 (1969).
[7] R. Kaptein and J. L. Oosterhoff, Chem. Phys. Lett. **4**, 195 (1969).
[8] E. Daviso *et al.*, J. Phys. Chem. C **113**, 10269 (2009).
[9] E. Daviso *et al.*, Proc. Natl. Acad. Sci. U. S. A. **106**, 22281 (2009).
[10] G. Jeschke and J. Matysik, Chem. Phys. **294**, 239 (2003).
[11] G. Jeschke, J. Am. Chem. Soc. **120**, 4425 (1998).
[12] G. Jeschke, J. Chem. Phys. **106**, 10072 (1997).
[13] T. Polenova and A. E. McDermott, J. Phys. Chem. B **103**, 535 (1999).
[14] S. Prakash *et al.*, J. Am. Chem. Soc. **127**, 14290 (2005).
[15] S. S. Thamarath *et al.*, J. Am. Chem. Soc. **134**, 5921 (2012).
[16] J. Matysik *et al.*, Proc. Natl. Acad. Sci. U. S. A. **97**, 9865 (2000).
[17] A. Diller *et al.*, Proc. Natl. Acad. Sci. U. S. A. **104**, 12767 (2007).
[18] Alia *et al.*, J. Am. Chem. Soc. **126**, 12819 (2004).
[19] D. V. Sosnovsky *et al.*, J. Chem. Phys. **144**, 144202 (2016).
[20] D. V. Sosnovsky *et al.*, J. Chem. Phys. **150**, 094105 (2019).
[21] E. Daviso *et al.*, J. Am. Chem. Soc. **133**, 16754 (2011).
[22] M. Najdanova *et al.*, Photochem. Photobiol. **94**, 69 (2018).
[23] M. G. Zysmilich and A. McDermott, J. Am. Chem. Soc. **116**, 8362 (1994).
[24] M. G. Zysmilich and A. McDermott, J. Am. Chem. Soc. **118**, 5867 (1996).
[25] E. Daviso, G. Jeschke, and J. Matysik, in *Biophysical Techniques in Photosynthesis*, edited by T. Aartsma and J. Matysik (Springer Netherlands, 2008), p. 385.
[26] E. Daviso *et al.*, Appl. Magn. Reson. **37**, 49 (2009).
[27] G. J. Janssen *et al.*, Appl. Magn. Reson. **42**, 57 (2012).
[28] J. C. Zill *et al.*, Photosynth. Res. **137**, 295 (2018).
[29] J. C. Zill *et al.*, Photosynth. Res. **140**, 151 (2019).
[30] S. Paul *et al.*, J. Phys. Chem. B **119**, 13897 (2015).
[31] E. A. M. Schulten *et al.*, Biochemistry **41**, 8708 (2002).
[32] S. Prakash *et al.*, Biochemistry **46**, 8953 (2007).
[33] S. Shochat *et al.*, Photosynth. Res. **40**, 55 (1994).
[34] J. Raap *et al.*, Anal. Biochem. **191**, 9 (1990).
[35] P. Hušek, J. Chromatogr. A **552**, 289 (1991).
[36] M. R. Fischer *et al.*, Biochemistry **31**, 11038 (1992).
[37] A. E. Bennett *et al.*, J. Chem. Phys. **103**, 6951 (1995).
[38] Y. Wei, A. C. de Dios, and A. E. McDermott, J. Am. Chem. Soc. **121**, 10389 (1999).
[39] J. Matysik *et al.*, Indian J. Biochem. Biophys. **37**, 418 (2000).
[40] G. Schreckenbach and T. Ziegler, Int. J. Quantum Chem. **60**, 753 (1996).
[41] G. Schreckenbach and T. Ziegler, Int. J. Quantum Chem. **61**, 899 (1997).
[42] S. K. Wolff and T. Ziegler, J. Chem. Phys. **109**, 895 (1998).
[43] S. K. Wolff *et al.*, J. Chem. Phys. **110**, 7689 (1999).
[44] G. te Velde, F. M. Bickelhaupt, E. J. Baerends, C. Fonseca Guerra, S. J. A. van Gisbergen, J. G. Snijders, and T. Ziegler, J. Comput. Chem. **22**, 931 (2001).
[45] C. Fonseca Guerra, J. G. Snijders, G. te Velde, and E. J. Baerends, "Towards an order-N DFT method," Theor. Chem. Acc. **99**, 391 (1998).
[46] ADF2019, *SCM*, Theoretical Chemistry (Vrije Universiteit, Amsterdam, The Netherlands, 2019), http://www.scm.com.
[47] M. Gaus, Q. Cui, and M. Elstner, J. Chem. Theory Comput. **7**, 931 (2011).
[48] M. Gaus, A. Goez, and M. Elstner, J. Chem. Theory Comput. **9**, 338 (2013).
[49] M. H. B. Stowell *et al.*, Science **276**, 812 (1997).
[50] S. Stoll and A. Schweiger, J. Magn. Reson. **178**, 42 (2006).
[51] F. Lendzian *et al.*, Biochim. Biophys. Acta, Bioenerg. **1183**, 139 (1993).
[52] E. Daviso *et al.*, in *Photosynthesis. Energy from the Sun*, edited by J. F. Allen *et al.* (Springer Netherlands, Dordrecht, 2008), p. 25.
[53] S. Prakash, S. H. Tong, A. Alia, P. Gast, H. J. M. de Groot, G. Jeschke, and J. Matysik, in *Proceedings of the 13th International Congress on Photosynthesis* (Allen Press, 2005), p. 236.
[54] T. Egorova-Zachernyuk *et al.*, Magn. Reson. Chem. **46**, 1074 (2008).
[55] L. Limantara *et al.*, Chem. Phys. Lett. **236**, 71 (1995).
[56] D. Gräsing, P. Bielytskyi, I. F. Céspedes-Camacho, A. Alia, T. Marquardsen, F. Engelke, and J. Matysik, Sci. Rep. **7**, 12111 (2017).